Stellar Wind-Blown Bubbles as Environments for Late-Time Rebrightening of Gamma-Ray Burst Afterglows

JIA REN , XIAO-YAN LI , YUN WANG , LU-LU ZHANG , DA-MING WEI , ZI-GAO DAI , ZHI-PING JIN , AND DA-BIN LIN 105

¹Purple Mountain Observatory, Chinese Academy of Sciences, Nanjing 210034, China ²Department of Astronomy, Xiamen University, Xiamen, Fujian 361005, China ³ College of Physics and Electronic Information Engineering, Guilin University of Technology, Guilin 541004, China ⁴Department of Astronomy, School of Physical Sciences, University of Science and Technology of China, Hefei 230026, China ⁵ Guanaxi Key Laboratory for Relativistic Astrophysics, School of Physical Science and Technology, Guanaxi University, Nanning 530004,

Submitted to ApJL

ABSTRACT

We presented the multi-wavelength afterglow fitting results for three events that exhibit late afterglow re-brightening behavior: EP240414a (z = 0.402), GRB 240529A (z = 2.695), and GRB 240218A (z = 6.782), which span a broad range of redshifts, from the local to the high-redshift universe. We prove that the peculiar afterglow light curves of three bursts can be well fitted by structured jets propagated in free-to-shocked stellar wind environment of stellar wind blown bubbles. This scenario offers a self-consistent explanation for the observed subclass of afterglows that exhibit rebrightening that characterized by steep rises and rapid decays. It also provides a unified solution for such events and offers pathways to study both the jet generation mechanism and the propagation process of jets through the envelope of progenitor. This study reveals that the structured jets produced by such events exhibit a narrow jet core and a steep angle-dependent energy decay index, suggesting highly magnetized jets. The derived transition radii from free stellar winds to shocked stellar winds for all three events are smaller than 0.5 pc, with statistical analysis of similar events indicating a median value of 0.1 pc, which conflicts with numerical simulation results. We anticipate that future observations by EP/SVOM missions will enhance the understanding of analogous events and further reveil information about progenitors and the circum-environments.

Keywords: Gamma-ray bursts (629); High energy astrophysics (739)

1. INTRODUCTION

Long gamma-ray bursts (LGRBs) have been observed in association with supernovae (Galama et al. 1998). Consequently, the progenitors of such events are widely thought to be massive stars at the end stages of their evolution, such as Wolf-Rayet (WR) stars and blue supergiant stars (Woosley & Bloom 2006). Such stars are generally considered to exhibit vigorous convective processes, possess extremely high surface temperatures,

Corresponding author: Da-Ming Wei, Jia Ren

dmwei@pmo.ac.cn renjia@pmo.ac.cn

drive powerful stellar winds, and may undergo episodic mass ejections. At the early times of the 21st century, it has been studied by utilizing numerical simulations and observations to delineate the specific structure of the wind-blown bubble surrounding the LGRB progenitor (Ramirez-Ruiz et al. 2001; Heyl & Perna 2003; Greiner et al. 2003; Chevalier et al. 2004; Ramirez-Ruiz et al. 2005; Eldridge et al. 2006; Pe'er & Wijers 2006; Chen et al. 2007; van Marle et al. 2008; Kong et al. 2010; Ramirez-Ruiz & MacFadyen 2010). The light curve behavior of LGRB afterglows effectively carries information about the radial evolution of the circumburst environment. This information, in turn, reflects the massejection history of the progenitor during its final evolutionary stages. It is theoretically expected that the cir-

cumburst environment of LGRBs to be wind-dominated, a scenario supported by some observational findings. However, the afterglow behaviors of many LGRBs can also be well explained by a circumburst environment consisting of a homogeneous medium. Futher, a series of studies based on early afterglow radiation indicates that the circumburst environment may be more complex, deviated from the typical stellar wind or uniform medium environment (e.g., Yi et al. 2013, 2020; Tian et al. 2022). In a word, the true nature of the circumburst environment remains highly uncertain (e.g., Heyl & Perna 2003; Monfardini et al. 2006).

In the accumulated observational data, there exists a significant number of GRB events exhibiting late-time afterglow rebrightening behavior, which proves difficult to explain using the standard afterglow models (e.g., Liang et al. 2013). During the same period, researchers often utilized the density jumps in the environment to explain the re-brightening phenomenon observed in the GRB afterglows (Ramirez-Ruiz et al. 2001; Dai & Lu 2002; Lazzati et al. 2002; Dai & Wu 2003; Tam et al. 2005; Gendre et al. 2007; Jin et al. 2009; Geng et al. 2014). Notably, Ramirez-Ruiz et al. (2001) and Eldridge et al. (2006) specifically calculated the corresponding afterglow light curves based on the windblown bubble simulation results; their findings reveal that when the jet propagates into the shocked-wind region, the afterglow displays distinct rebrightening features (however, see Nakar & Granot 2007; van Eerten et al. 2009, 2010; Gat et al. 2013).

Recently, the Einstein Probe (EP) satellite detected a series of transient events and their afterglows which identified as fast X-ray transients (FXTs). Owing to rapid post-trigger multi-wavelength follow-up observations, several FXTs detected by EP have been confirmed as GRBs. This suggests the existence of a distinct population among GRBs lack of gamma-ray emission but fruitful in X-ray band (e.g., Levan et al. 2024; Gillanders et al. 2024; Srivastav et al. 2025; van Dalen et al. 2025; Bright et al. 2025; Sun et al. 2025). We note that some of FXT afterglows exhibit late-time rebrightening behavior, e.g., EP240414a (Sun et al. 2025; van Dalen et al. 2025; Srivastav et al. 2025), and EP241021a (Shu et al. 2025; Busmann et al. 2025). This phenomenon occurs simultaneously in both X-ray and optical bands, showing rapid decay following a brief brightening phase. We realize that similar phenomena have also been observed past in many GRB afterglows (e.g., Laskar et al. 2015). They were usually interpreted by late energy injection (e.g., Zhang & Mészáros 2002; Björnsson et al. 2004; Geng et al. 2013; Hou et al. 2014; Laskar et al. 2015; Yu et al. 2015), refreshed shocks (e.g., Rees &

Mészáros 1998; Panaitescu et al. 1998; Granot et al. 2003; Sun et al. 2024; Geng et al. 2025) the radiation of e^{\pm} pairs in the relativistic wind bubble (Yu & Dai 2007; Geng et al. 2016), density jumps of the medium, and two or more component jets (e.g., Huang et al. 2004; Guidorzi et al. 2005; Starling et al. 2005; Filgas et al. 2011; Nardini et al. 2011, 2014).

We remind that the temporal slopes before and after the rebrightening typically differ significantly, with a flatter slope in the pre-phase and a steeper slope in the after-phase. The time decay slope after the rebrightening is generally close to the typical jet-break. The commonality demonstrated by such events remind that they might be driven by the same physical mechanisms and be related to the jet itself.

In this Letter, we studied three recent events, EP240414a, GRB 240529A, and GRB 240218A. They exhibit the simultaneous late multi-wavelength afterglow brightening behavior. Our research indicates that such events can actually be jointly explained within the framework of wind-blown bubbles, and provides a unified paradigm for similar events.

This paper is organized as follows. We introduce the acquisition and usage of data in Section 2. In Section 3, we introduce our model considerations. In Section 4, we briefly discuss with analytical derivations how the rebrightening behavior occurs. In Section 5, we introduce our fitting parameters and method in detail. The results of model parameter inference and corresponding discussion are presented in Section 6. We summarize and conclusion the significance of our results in Section 7. We take the cosmology parameters as $H_0 = 67.8 \text{ km s}^{-1} \text{ Mpc}^{-1}$, and $\Omega_M = 0.308 \text{ (Planck Collaboration et al. 2016)}$.

2. THE ACQUISITION AND USAGE OF DATA

For EP240414a, we collected data from Bright et al. (2025), van Dalen et al. (2025), Srivastav et al. (2025), Sun et al. (2025) and neglected the optical data later than 10 days which dominated by supernova. For GRB 240529A, we collected data from Swift data center, Sun et al. (2024) and reference therein. For GRB 240218A we use data from Swift data center and Brivio et al. (2025).

3. MODEL ASSUMPTION

In this work, we used the state-of-art package ASGARD to generate multi-wavelength afterglow light curves (Ren et al. 2024, see appendix for details). We have numerically solved forward shock dynamics (Nava et al. 2013; Zhang 2018). The time-dependent electron continuity equation is solved with first-order accuracy which

includes the accurate inverse Compton cooling effect (Nakar et al. 2009). We accounted for synchrotron radiation and considered the equal-arrival-time surface effect accordingly (Waxman 1997).

3.1. Jet Structure

We consider an axisymmetric structured jet model for bursts and employed a two-part function to describe the shape of the jet,

$$\begin{cases} E_{k,iso}(\theta) = E_{k,iso,0}, \ \Gamma(\theta) = \Gamma_0, & \theta \leqslant \theta_c, \\ E_{k,iso}(\theta) = E_{k,iso,0} \left(\frac{\theta}{\theta_c}\right)^{k_E}, \ \Gamma(\theta) = \Gamma_0 \left(\frac{\theta}{\theta_c}\right)^{k_\Gamma}, & \theta_j \geqslant \theta > \theta_c, \end{cases}$$

$$(1)$$

where $E_{\rm k,iso}(\theta)=4\pi\varepsilon(\theta)$ is the isotropic kinetic energy of jet with $\varepsilon(\theta)$ being the energy per unit solid angle, and $\Gamma(\theta)$ is the initial bulk Lorentz factor, respectively. We artificially set a minimum value of 1.4 for $\Gamma(\theta)$, corresponding to $\beta\simeq 0.7$. The fitting results presented in this work all meet $\Gamma(\theta_{\rm j})>1.4$. In many works, the form of a broken powerlaw function as

$$\{E_{\rm k,iso}(\theta), \Gamma_0(\theta)\} \propto \left(1 + \frac{\theta}{\theta_{\rm c}}\right)^{\{k_E, k_\Gamma\}}$$
 (2)

is adopted. We point out that this form leads to the strong degeneracy of the core opening angle θ_c and the attenuation exponent k_{Γ} and k_E of the jet. The smooth transition between the core and peripheral regions actually hinders a better limitation of the attenuation index and the viewing angle.

The specific flux calculation is performed based on discretized grids along the (θ, ϕ) dimensions. The minimum size $(\delta\theta, \delta\phi)$ of the radiation patch is determined by $\delta\theta = \delta\phi \ll 1/\Gamma_0$.

3.2. Circum-Burst Environment

For massive stars accompanied by long GRBs, stellar winds are expected to form. The structure of their stellar wind bubble has been studied extensively (e.g., Castor et al. 1975; Scalo & Wheeler 2001; Eldridge et al. 2006). It is generally believed that four regions are formed when stellar winds interact with the interstellar medium (ISM), namely the free stellar wind, the shocked wind, the shocked ISM, and the unshocked ISM (Pe'er & Wijers 2006). The number density of the free stellar wind medium is given by $n_f = 3 \times 10^{35} A_{\star} r^{-2} \text{cm}^{-1}$, where A_{\star} is a constant known as the wind parameter (Chevalier & Li 2000). The number density of the free-to-shocked wind environment is described as

$$n(r) = \begin{cases} n_f(r), & r < R_{\rm tr}, \\ n_s = \xi n_f(R_{\rm tr}), & r \geqslant R_{\rm tr}, \end{cases}$$
 (3)

where $R_{\rm tr}$ is the transition radius of the circum-burst environment from free to shocked wind, and $\xi = \frac{(\hat{\gamma}+1)\mathcal{M}_{\rm wind}^2}{(\hat{\gamma}-1)\mathcal{M}_{\rm wind}^2+2} = 4$ is adopted in this paper, where we take $\hat{\gamma} = 5/3$ for stellar wind and the Mach number $\mathcal{M}_{\rm wind} \gg 1$.

4. ANALYTICAL EXPLANATION FOR AFTERGLOW REBRIGHTING

Based on Li et al. (2021), we briefly discuss how the rebrightening behavior occurs. The derivations based on the external-forward shock dynamics of a tophat jet with its half-opening angle as $\theta_{\rm j}$. The specific frequencies $\nu_{\rm m}$ and $\nu_{\rm c}$, and the peak spectral flux $F_{\nu,\rm max}$ can be calculated. For on-axis viewer ($\theta_{\rm v} < \theta_{\rm j}$),

$$\begin{cases} \nu_{\rm c} \propto \bar{\Gamma}_{\rm obs}^{8} \left[n \left(\bar{r}_{\rm obs} \right) \right]^{3/2} \bar{r}_{\rm obs}^{-2}, \\ \nu_{\rm m} \propto \bar{\Gamma}_{\rm obs}^{4} \left[n \left(\bar{r}_{\rm obs} \right) \right]^{1/2}, \\ F_{\nu, \rm max} \propto \kappa \bar{\Gamma}_{\rm obs}^{2} \left[n \left(\bar{r}_{\rm obs} \right) \right]^{3/2} \bar{r}_{\rm obs}^{3}; \end{cases}$$
(4)

and for off-axis viewer $(\theta_{\rm v} > \theta_{\rm i} + 1/\bar{\Gamma})$,

$$\begin{cases} \nu_{\rm c} \propto \bar{\Gamma}_{\rm obs}^{6} \left[n \left(\bar{r}_{\rm obs} \right) \right]^{3/2} \bar{r}_{\rm obs}^{-2}, \\ \nu_{\rm m} \propto \bar{\Gamma}_{\rm obs}^{2} \left[n \left(\bar{r}_{\rm obs} \right) \right]^{1/2}, \\ F_{\nu,\rm max} \propto \kappa \bar{\Gamma}_{\rm obs}^{-2} \left[n \left(\bar{r}_{\rm obs} \right) \right]^{3/2} \bar{r}_{\rm obs}^{3}, \end{cases}$$
(5)

where $\kappa = \left\{1 - 1/\left\{1 + 2\bar{\Gamma}^2 \left[1 - \cos\left(\theta_{\rm j} + \theta_{\rm v}\right)\right]\right\}^2\right\}$, $\bar{\Gamma}_{\rm obs}$ and $\bar{r}_{\rm obs}$ are the Lorentz factor and the shock front radius of the jet flow closest to the light of sight. Besides, the evolution of jet dynamics is

$$\begin{cases} \text{for } \bar{r}_{\text{obs}} < R_{\text{dec}}: \\ \bar{\Gamma}_{\text{obs}} = \text{const}, \bar{r}_{\text{obs}} \propto t_{\text{obs}}; \\ \text{for } \bar{r}_{\text{obs}} > R_{\text{dec}}, k = 2, \text{ and } \theta_{\text{v}} < \theta_{\text{jet}}: \\ \bar{\Gamma}_{\text{obs}} \propto t_{\text{obs}}^{-1/4}, \bar{r}_{\text{obs}} \propto t_{\text{obs}}^{1/2}; \\ \text{for } \bar{r}_{\text{obs}} > R_{\text{dec}}, k = 2, \text{ and } \theta_{\text{v}} > \theta_{\text{jet}} + 1/\bar{\Gamma}: \\ \bar{\Gamma}_{\text{obs}} \propto t_{\text{obs}}^{-1/2}, \bar{r}_{\text{obs}} \propto t_{\text{obs}}; \\ \text{for } \bar{r}_{\text{obs}} > R_{\text{dec}}, k = 0, \text{ and } \theta_{\text{v}} < \theta_{\text{jet}}: \\ \bar{\Gamma}_{\text{obs}} \propto t_{\text{obs}}^{-3/8}, \bar{r}_{\text{obs}} \propto t_{\text{obs}}^{1/4}; \\ \text{for } \bar{r}_{\text{obs}} > R_{\text{dec}}, s = 0, \text{ and } \theta_{\text{v}} > \theta_{\text{jet}} + 1/\bar{\Gamma}: \\ \bar{\Gamma}_{\text{obs}} \propto t_{\text{obs}}^{-3/2}, \bar{r}_{\text{obs}} \propto t_{\text{obs}}, \end{cases}$$

where $R_{\rm dec}$ is the deceleration radius of jet, and k=2 corresponding to free wind medium, k=0 for uniform medium, respectively. Basing on the results of Sari et al. (1998), and adopt the observed spectral flux f_{ν} ($t_{\rm obs}$) $\propto t_{\rm obs}^{-\alpha} \nu^{-\beta}$, then the closure relations between α and β can be derived (e.g., Zhang & Mészáros 2004; Zhang et al. 2007)

For the optical afterglow, the typical scenario considers the $\nu_{\rm m} < \nu_{\rm opt} < \nu_{\rm c}$ under slow cooling conditions. If

the jet is in the coasting phase while sequentially traversing both the free stellar wind and the uniform medium, i.e., $\bar{r}_{\rm obs} < R_{\rm dec}$, then one can have $\alpha = (p-1)/2$ (wind) and $\alpha = -3$ (uniform), where $p \in (2,3)$ is the powerlaw index of shock-accelerated nonthermal electrons. It is effective both for on-axis and off-axis secnario. Another possible scenario is when jet is decelerated, $\bar{r}_{\rm obs} > R_{\rm dec}$, and is off-axis-observed. One can derive $\alpha = p - 2$ (wind) and $\alpha = -(15-3p)/2$ (uniform). In both scenarios, the optical afterglow can exhibit a transition from gradual decay to rapid brightening, naturally explaining the rebrightening slopes ranging from t^3 to $t^{4.5}$. This aligns remarkably well with the observational data from the two EP events EP240414a (t^3 , Zheng et al. 2025) and EP241021a (t^4 , Busmann et al. 2025). There are other scenarios that can produce rebrightening behavior, please see Li et al. (2021) for more details.

Spectroscopic observations during rebrightening phases can provide crucial diagnostics on the nature of the radiating region. For instance, given its triggering as a FXT by EP and its association with a supernova, the rebrightening of EP240414a is widely attributed to the radiation from a cocoon cooling process. However, the spectroscopic of EP240414a is non-thermal dominated (Srivastav et al. 2025; van Dalen et al. 2025). Besides, similar rebrightening behaviors have also been observed in typical GRBs and high-redshift GRB events.

As typical cases, the three events selected in this study, EP240414a (z=0.402), GRB 240529A (z=2.695), and GRB 240218A (z=6.782), span a broad range of redshifts, from the local to the high-redshift universe. The most prominent common feature among these events is the presence of a distinct jet-break phase immediately following the rebrightening episode. A successful picture should self-consistently explain the commonalities revealed in the data, and the model of structured jet traversing stellar wind bubbles achieves precisely this.

5. FITTING METHOD AND RESULTS

5.1. Fitting Method

We perform posterior parameter inference using the Markov Chain Monte Carlo (MCMC) technique, employing the Python package emcee as the sampler (Foreman-Mackey et al. 2013). The sampling was carried out in multi-dimensional parameter space. The basic model parameters include $\{n_s, A_{\star}, E_{\rm k,iso}, p, \Gamma_0, \epsilon_e, \epsilon_B, \xi_e, \theta_c, \theta_{\rm j}, \theta_{\rm v}, k_{\Gamma}, k_E\}$, where $\epsilon_e, \epsilon_B, \xi_e$, are the energy fraction of electrons and magnetic field in the jet and the number fraction of nonthermal electrons, respectively. We also considered the extinction from host galaxies. For simplicity, we invoked the extinction

package (Barbary 2016) in our fitting program and setting $E(B-V)_{\rm host}$ and $R_{V,\rm host}$ as fitting parameters. According to Sun et al. (2025), we ignored the extinction of host galaxy of EP240414a; besides, Brivio et al. (2025) find $E(B-V)_{\rm host}=0.12$ for GRB 240218A when assuming SMC-like extinction law; for GRB 240529A, both parameters are inferred by the fitting. After discarding the burn-in stage, the resulting marginalized posterior probability density distributions are presented in Appendix, Figure 4 for EP240414a, Figure 5 for GRB 240529A, and Figure 6 for GRB 240218A, respectively. The corresponding parameter values obtained are detailed in Table 1.

5.2. Basic results

We find relativity low wind parameter of all three bursts $A_{\star} \sim 0.1$, consistent with the WR progenitor scenario. The kinetic energy of these bursts are located in the high level of energy distribution of GRBs. For the two typical GRBs, GRB 240529A has isotropicequivalent prompt emission energy $E_{\gamma,\rm iso} = 2.2^{+0.7}_{-0.8} \times$ 10⁵⁴ erg (Svinkin et al. 2024), in turn, the prompt emission efficiency is $\eta_{\gamma} = E_{\gamma,iso}/(E_{\gamma,iso} + E_{k,iso}) \sim 5.7\%;$ GRB 240218A has $E_{\gamma,\rm iso} \sim 3.24 \times 10^{53}$ erg (Brivio et al. 2025), thus $\eta_{\gamma} \sim 0.8\%$. We note that in our fittings, GRB 240529A is observed in jet core $(\theta_v/\theta_c \sim 0.14)$ but GRB 240218A is off-axis-viewed ($\theta_{\rm v}/\theta_{\rm c} \sim 2.28$). Thus the relatively low radiation efficiency of GRB 240218A can be understood. EP240414a has a very low $E_{X,\rm iso} \sim 5.3^{+1.2}_{-0.9} \times 10^{49} \text{ erg in } 0.5 - 4 \text{ keV band (Sum}$ et al. 2025). Although the fitting yields an isotropicequivalent kinetic energy $E_{\rm k,iso} \sim 2 \times 10^{54}$ erg, this scenario remains highly self-consistent due to the extremely large off-axis viewing angle ($\theta_{\rm v}/\theta_{\rm c} \sim 8.25$).

The bulk Lorentz factors of these bursts are typical, the median distribution values of EP240414a and GRB 240529A are both $\Gamma_0 \sim 100$, and for GRB 240218A $\Gamma_0 \sim 316$. For all three bursts we observe very narrow core opening angle $\theta_{\rm c} \sim 0.01$ rad. We will give possible explanation in Section 6.1 in detail. We get typical ϵ_e and ϵ_B . The accelerated electron fraction ξ_e of all three bursts are higher than 0.3, indicate high acceleration efficiencies of them.

5.3. Transition Radius

The transition radius, where is the inner radius of the terminal shock of wind, can be calculated with $n_s = \xi n_f(R_{\rm tr}) = 3 \times 10^{35} A_{\star} R_{\rm tr}^{-2} \xi$. Thus $R_{\rm tr} = 1.1 \times 10^{18} A_{\star}^{1/2} n_s^{-1/2}$ cm. The best-fit results of $R_{\rm tr}$ are listed in Table 2, we find all three bursts have small transition radius < 0.5 pc. We also collected some bursts that were considered to involve free-to-shocked wind conversion behaviors and listed them in Table 2. One can

			7				
Parameter	$Range^{a}$	Value^{b}					
		EP240414a	GRB 240529A	GRB 240218A			
$\frac{\log_{10} n_s \text{ (cm}^{-3})}{}$	[-3, 0]	$-0.75^{+0.29}_{-0.30}$	$-0.68^{+0.10}_{-0.13}$	$-0.22^{+0.13}_{-0.27}$			
$\log_{10} A_{\star}$	[-3, 0]	$-0.56^{+0.44}_{-0.18}$	$-0.81^{+0.10}_{-0.08}$	$-0.71^{+0.08}_{-0.13}$			
$\log_{10} E_{\rm k,iso} \ ({\rm erg})$	[53.5, 56.5]	$54.30^{+0.19}_{-0.16}$	$55.56^{+0.13}_{-0.05}$	$55.59^{+0.13}_{-0.12}$			
p	[2, 3]	$2.26^{+0.02}_{-0.04}$	$2.11^{+0.01}_{-0.01}$	$2.22^{+0.04}_{-0.04}$			
$\log_{10}\Gamma_0$	[1.5, 3]	$2.00^{+0.17}_{-0.11}$	$2.00^{+0.01}_{-0.01}$	$2.50^{+0.06}_{-0.09}$			
$\log_{10} \epsilon_e$	[-3, -0.5]	$-1.48^{+0.15}_{-0.21}$	$-1.49^{+0.04}_{-0.08}$	$-1.44^{+0.11}_{-0.12}$			
$\log_{10} \epsilon_B$	[-6, -0.5]	$-1.72^{+0.23}_{-0.32}$	$-1.77^{+0.07}_{-0.10}$	$-3.92^{+0.25}_{-0.19}$			
$\log_{10} \xi_e$	[-3, 0]	$-0.32^{+0.16}_{-0.21}$	$-0.46^{+0.07}_{-0.08}$	$-0.20^{+0.09}_{-0.08}$			
$\log_{10} \theta_{\rm c} \ ({\rm rad})$	[-3, 0]	$-1.97^{+0.11}_{-0.05}$	$-2.12^{+0.01}_{-0.07}$	$-2.10^{+0.06}_{-0.06}$			
$\log_{10}(\theta_{\mathrm{j}}/\theta_{\mathrm{c}})$	[0, 1]	$0.43^{+0.14}_{-0.12}$	$0.64^{+0.03}_{-0.06}$	$0.55^{+0.16}_{-0.06}$			
$ heta_{ m v}/ heta_{ m c}$	[0, 10]	$8.25^{+0.57}_{-1.08}$	$0.14^{+0.07}_{-0.05}$	$2.28^{+0.19}_{-0.18}$			
k_{Γ}	[-8, 0]	$-3.34^{+0.35}_{-1.17}$	$-1.32^{+0.09}_{-0.09}$	$-0.25^{+0.18}_{-0.30}$			
k_E	[-8, 0]	$-7.54^{+1.06}_{-0.31}$	$-4.69^{+0.19}_{-0.17}$	$-4.40^{+0.51}_{-0.64}$			
$E(B-V)_{ m host}$	[0, 1]	0(fixed)	$0.65^{+0.03}_{-0.02}$	0.12 (fixed)			
$R_{V, ext{host}}$	[1, 5]	_	$2.74^{+0.09}_{-0.13}$	2.93(SMC)			
$R_{\rm tr}~({\rm cm})$	=	13.63×10^{17}	9.43×10^{17}	6.23×10^{17}			

Table 1. Fitting Results

observe all sample values are less than 1 pc. By fitting those logarithmic distribution with a Gaussian function, we found that the median value is $\log_{10}R_{\rm tr}({\rm cm})=17.63$, with a standard deviation STD=0.47, as shown in Figure 2.

Based on the different progenitor stars and the properties of the burst environment, recently Chrimes et al. (2022) conducted a systematic study on the characteristics of the stellar wind bubbles around long GRBs through a series of numerical simulations. Their statistic results indicate that the median value of the wind termination shock radius is located at 10 pc. Thus, the above results indicate that the inferred conversion radius based on observations shows a systematic deviation from the numerical simulation results. The exact cause of this deviation remains unknown. However, we hypothesize that one possible explanation is that the GRB progenitors are extremely unstable and collapsed during the early stage of rapid mass loss process, preventing the stellar wind bubble from expanding to the size predicted by the numerical simulation (e.g., Ramirez-Ruiz et al. 2005). Besides, the simulation results are taken place in one dimensional, the instability that only occurs in high-dimensional situations, e.g., Rayleigh-Taylor and Kelvin-Helmholtz Instabilities, may lead to a smaller transition radius.

In Figure 3, we present the correlation between the transition radii $R_{\rm tr}$ and the transition times $T_{\rm tr}$. We define $T_{\rm tr}$ as the onset moment when the broadband light curve exhibits rebrightening behavior. The specific values are also listed in the Table 2. For the convenience of analysis, we also provide the redshift and off-axis factor $\theta_{\rm v}/\theta_{\rm c}$ of each event. We point out that since the rebrightening takes place in a uniform medium environment (see Section 4), the occurrence time of rebrightening can be described by the following relation (e.g., Beniamini et al. 2020, Equation 31),

$$T_{\rm tr} \propto \left(\frac{\theta_{\rm v}}{\theta_{\rm c}}\right)^{\frac{2(4-k)}{3-k}} = \begin{cases} \left(\theta_{\rm v}/\theta_{\rm c}\right)^{8/3}, & \theta_{\rm v} \ge \theta_{\rm c}; \\ 1, & \theta_{\rm v} < \theta_{\rm c}. \end{cases}$$
(7)

After taking into account the redshift correction, we apply the above relationship to convert the transition time into the on-axis situation. We also plot reference lines to characterize the relationship between the propagation distance of GRB jets in a wind-like medium and time (Granot & Sari 2002),

$$R = \left[\frac{(17 - 4k)(4 - k)E_{k,iso}t'}{4\pi Ac} \right]^{1/(4-k)}, \tag{8}$$

where $A = 5 \times 10^{11} \mathrm{g \ cm^{-1}} A_{\star}$, and take k = 2. Basing on a log-linear function fit we find the corrected samples

 $[^]a$ Uniform prior distribution.

^b Errors in 1σ .

REN ET AL.

follows the relation as

$$\log_{10} R_{\rm tr}(\rm cm) = 0.56 \log_{10} T_{\rm tr} + 16.24. \tag{9}$$

It can be clearly see that samples follow the 1/2 slope expected for a wind environment, rather than the 1/4 slope characteristic of a homogeneous environment.

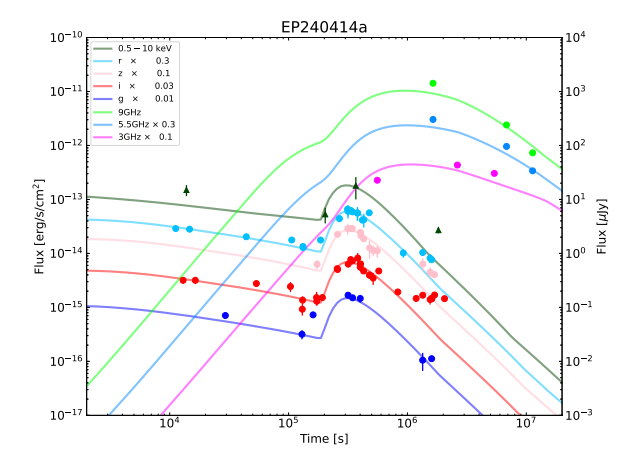
6. DISCUSSION

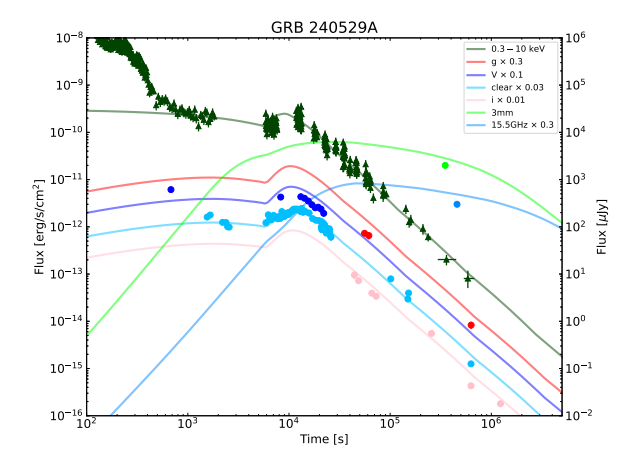
6.1. Jet Structure

Very narrow jet core with $\theta_{\rm c} \sim 0.01$ rad has obtained for all three bursts in this work. In the model adopted in this paper, narrower jets facilitate the production of more sharper rebrightening features, transitioning directly from the peak flux phase to the jet-break stage, as demonstrated in Figure 3 of Li et al. (2021). Besides, Li et al. (2021) also suggest small θ_c of GRBs 120326A, 100901A, 100814A, and 120404A. Although their structured jet model was an Gaussian jet, we suppose both results have comparability due to the very sharp jet edge from our work. Such small θ_c are rare but has existed in the BOAT GRB 221009A which provides circumstantial evidence for our results. Narrow jets may not be uncommon in GRBs. Some bright X-ray flares comparable to or even stronger than the prompt emission (e.g., Falcone et al. 2006) could be emitted by narrow jets slightly offset from the line of sight. Observers would typically miss the prompt emission of narrow jet entirely in most cases. Under this scenario, most GRBs are observed within the wing of structured jet (Zhang et al. 2024).

The relativistic jets that successfully break out from the progenitor's envelope can indeed produce very narrow jet opening angles. The post-breakout jet opening angle, θ_i , depends on the initial jet opening angle θ_0 injected by the black hole into the progenitor's envelope, the jet power, and the progenitor's radius and density profile. For relativistic hydrodynamical jet, one can find $\theta_i/\theta_0 \sim 1/10$ can be easy to achieve (Hamidani & Ioka 2021, Equation 35). However, the realistic value of θ_0 is uncertain, and it is often assumed in literatures that $\theta_0 \sim 10^{\circ}$, so that $\theta_i \sim 1^{\circ}$ is natural. For magnetized jets, the powerful pinch effect from well-ordered magnetic fields helps protect the relativistic jet from severe baryon contamination by the cocoon material and confines the jet to smaller opening angles (Gottlieb et al. 2020). Consequently, magnetically dominated jets are more promising to possess narrower jet cores.

Basing on the fitting results, we have the angular distribution indexes of jet structure as $k_{\Gamma} = -3.34^{+0.35}_{-1.17}$, $-1.32^{+0.09}_{-0.09}$, $-0.25^{+0.18}_{-0.30}$; $k_E = -7.54^{+1.06}_{-0.31}$, $-4.69^{+0.19}_{-0.17}$, $-4.40^{+0.51}_{-0.64}$, for EP240414a, GRB 240529A, and GRB 240218A, respectively. All bursts possess highly relativistic jets and exhibit a pronounced attenuation of





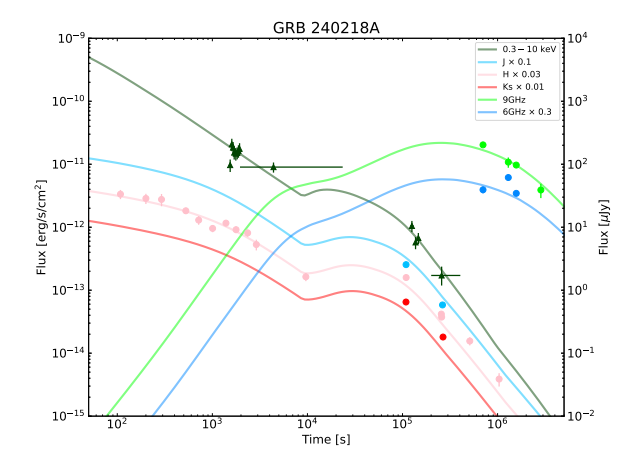


Figure 1. The best-fit light curves for the three events. From top to bottom: a local low-luminosity burst EP240414a, a typical nearby GRB 240529A, and a high-redshift GRB 240218A, respectively. The X-ray flux uses the Y-axis on the left, while other bands use the Y-axis on the right.

•

Transients	Transition Radius	Transition Time	$\theta_{ m v}/\theta_{ m c}$	redshift	Reference
	$(\times 10^{17} \mathrm{cm})$	(s)			
GRB 050319	(3.0 - 15.0)	1700	0	3.24	Kamble et al. (2007)
GRB $081109A$	4.5	300	0	0.98	Jin et al. (2009)
GRB $100814A$	4.0	18000	3.66	1.44	Li et al. (2021)
GRB $100901A$	1.9	9000	4.50	1.408	Li et al. (2021)
GRB $120326A$	1.0	4000	4.14	1.798	Li et al. (2021)
$\mathrm{GRB}\ 120404\mathrm{A}$	0.63	900	0.68	2.876	Li et al. (2021)
GRB $140423A$	4.1	5000	0	3.26	Li et al. (2020)
$\mathrm{GRB}\ 160625\mathrm{B}$	26.0	8000	0	1.406	Fraija et al. (2017)
GRB $190114C$	2.3	400	0	0.424	Fraija et al. (2019)
EP240414a	13.6	150000	8.25	0.402	this work
GRB $240529A$	9.4	7000	0.14	2.695	this work
GRB $240218A$	6.2	10000	2.28	6.782	this work

Table 2. Possible Free-to-Shocked Wind Environment Transients

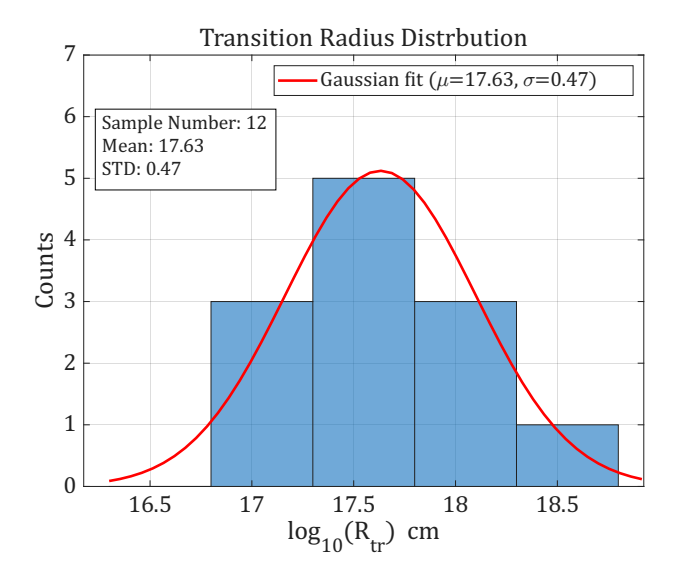


Figure 2. Transition radius distribution of samples, fitted by a lognormal function.

the wing component in their energy distribution, which aligns well with the results of numerical simulations. It is evident that k_{Γ} and k_{E} exhibit significant variations across different bursts. However, we point out that $\Gamma(\theta) \propto E_{\rm k,iso}(\theta)/M_{\rm jet}(\theta)c^2$, thus the angle-dependent mass distribution index $k_{M}=k_{E}-k_{\Gamma}$ characterizes the distribution of baryon loading in the jet. It is easy to derive that k_{M} approximates range in (-3,-4), distributed within a relatively narrow range. This result characterizes the mixing intensity of matter at the interface within the jet-cocoon system and from the jet head region, potentially hinting at the mechanisms of jet-cocoon interactions within collapsar.

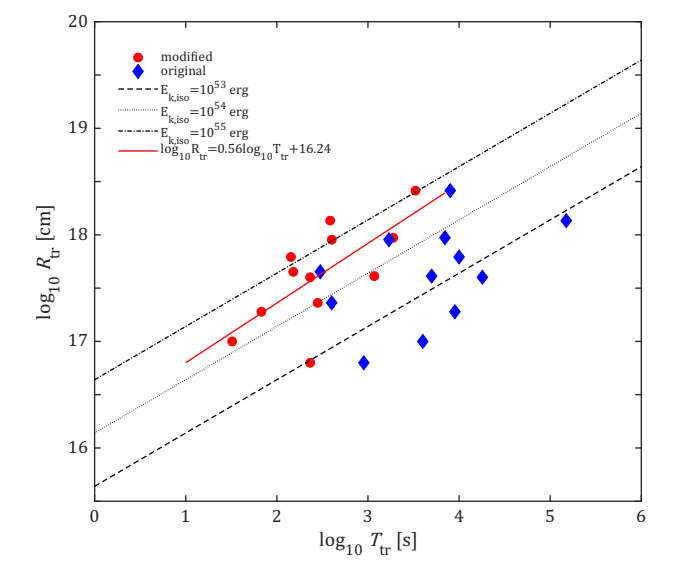


Figure 3. The correlation between the transition radii $R_{\rm tr}$ and the transition times $T_{\rm tr}$. The blue diamonds represent the observed values without considering redshift and viewing angle corrections from Equation 7, while the red dots show the corrected results. The dashed, solid, and dash-dotted lines correspond to the relationships between jet propagation distance and time under different jet kinetic energies, respectively. The results are calculated according to Equation 8, where we have taken $A_{\star}=0.3$.

Numerical simulations of jets based on relativistic magnetohydrodynamics (RMHD) often show the jet exhibits steep decay slopes in energy and Lorentz factor beyond θ_c . Based on Tchekhovskoy et al. (2008), $k_E < -4$, potentially reaching down to -10; k_Γ may have a two-segment structure ranging from gentle to steep, transitioning from -1 to -2.5. We note that the

fitting results presented in this work are consistent with the results of RMHD jet simulations.

6.2. Fomation Rate

Rastinejad et al. (2025) estimated the occurrence rate of FXT events is at least few $\times 10 \text{ Gpc}^{-3} \text{ yr}^{-1}$, which is higher than the typical high luminosity GRBs rate of $\sim 1 \; \rm Gpc^{-3} \; yr^{-1}$ (Sun et al. 2015). Sun et al. (2025) also inferred a local event rate density similar to EP240414aas $< 1 \text{ Gpc}^{-3} \text{ yr}^{-1}$, and upper limit for FXT events without gamma-ray counterparts as $< 10 \text{ Gpc}^{-3} \text{ vr}^{-1}$. Based on the model presented in this paper, it can be naturally attributed to the off-axis observation of the jet. On the one hand, based on the fitting result, the EP240414a event can still be observed by EP when $\theta_{\rm v} > 8\theta_{\rm c}$. From this, it can be roughly estimated that the observation rate of similar events can reach several tens of times that of typical GRB events, matching the results inferred by Rastinejad et al. (2025). Under the scenario of off-axis jet observations, FXT events without gamma-ray counterparts correspond to cases with extremely large viewing angles, representing a subclass of off-axis-viewed events. Meanwhile, the detection is also constrained by instrumental selection effects, hence the actual event rate should be lower than our rough estimate. On the other hand, we constrained the energy decay slope of the structured jet's power-law wing to be more sharp than θ^{-4} , result in the jet closer to a tophat structure. The lack of gamma-ray radiation can be coherently explained within this framework, thus also implies that such events likely originate from off-axisviewed GRBs.

7. SUMMARY AND CONCLUSION

The recently discovered series of novel X-ray sources by EP have garnered widespread attention due to their uniquely long duration timescales and anomalously low peak energies. The multi-wavelength optical counterparts of these events (represented by EP240414a and EP241021a) often exhibit sudden rebrightening phenomena. Current theoretical models frequently discuss scenarios involving large-angle outflow afterglows (cocoon or structured jet wings, Gianfagna et al. 2025; Yadav et al. 2025), refreshed shocks (Busmann et al. 2025; Srivastav et al. 2025), multiple single-component jets (triple jets, Shu et al. 2025; wobbling jets, Gottlieb 2025), thermal-dominated cooling radiation (cocoon/shocked ejecta, van Dalen et al. 2025; Hamidani et al. 2025; Sun et al. 2025; Zheng et al. 2025), or merger/accretion induced collapse remnant interiors with magnetized wind nebula (also thermal-dominated, Wu et al. 2025).

The aforementioned models have achieved their respective successes in interpreting the observational data from different perspectives. However, upon reviewing the historical observations and literature of typical GRBs, it is not uncommon to encounter similar latetime rebrightenings in the optical afterglow. In the past, these have always been explained as energy injections, refreshed shocks, relativistic wind bubbles, density jumps, and multi-component jets. This paper does not intend to debate the merits and demerits of the above-mentioned models. Instead, we attempt to take a holistic view and attempt to establish a more universal model that is applicable across different redshifts, progenitor star properties, jet structures, and viewing angles. In this work, we demonstrate the possibility of such a more unified picture through three distinctive events. A structured jet produced by the collapse of a massive star—potentially magnetized—is propagate through the wind-blown bubble surrounding the progenitor star. The sudden rebrightening behavior of the afterglow occurs when the jet shocks pass through the terminal shock region of the stellar wind. This scenario offers a self-consistent explanation for the observed subclass of afterglows that exhibit rebrightening, characterized by steep rises and rapid decays.

The transition of circum-jet environment from the free wind region to the shocked wind region does not necessarily involve a complete deceleration of the jet. Specifically, the model just needs that the Lorentz factor of the jet during rebrightening coincides with the opening angle of the jet core $1/\Gamma(t_{\rm obs}) \sim \theta_{\rm c}$, thereby producing the peculiar afterglow behavior. When other parameters are held constant, variations in the viewing angle and jet structure can naturally shift the afterglow light curve from classical behavior to a late rebrightening pattern. Furthermore, even for an on-axis observer, rebrightening features may still arise when specific physical parameters are considered, e.g., the deceleration radius of jet exceeds the transition radius of wind bubble, corresponding to weaker stellar winds and denser ISM. These have been unequivocally demonstrated by Li et al. (2021).

Considering potential variations in the wind strength and stochastic mass ejection processes of progenitor, the wind bubble may exhibit complex radial density structures. Under such conditions, the afterglow light curve could display even more intricate behaviors. We plan to conduct targeted numerical calculations to model these more complex scenarios. In the future, we hope to further validate the reliability of this framework by delving deeper into historical data and utilizing more observational data from EP/SVOM missions.

Software: Matplotlib (Hunter 2007), NumPy (Harris et al. 2020), emcee (Foreman-Mackey et al. 2013), corner (Foreman-Mackey 2016), Astropy (The Astropy Collaboration et al. 2013), extinction (Barbary 2016), SciPy (Virtanen et al. 2020),

ACKNOWLEDGMENTS

J. R. is Supported by the Postdoctoral Fellowship Program and China Postdoctoral Science Foundation (grant No. BX20250160), the Jiangsu Funding Program for Excellent Postdoctoral Talent (grant No. 2025ZB272), and the General Fund of the China Postdoctoral Science Foundation (grant No. 2024M763530). D.M.W. is supported by the Strategic Priority Research Program of the Chinese Academy of Sciences (grant No. XDB0550400), the National Key Research and Development Program of China (No. 2024YFA1611704), and the National Natural Science Foundation of China (NSFC; No. 12473049). Z.G.D. is supported by the NSFC under No. 12393812. Z.P.J. is supported by the NSFC under No. 12225305. D.B.L. is supported by the NSFC under No. 12273005. Y.W. is supported by the Jiangsu Funding Program for Excellent Postdoctoral Talent (grant No. 2024ZB110), the Postdoctoral Fellowship Program (grant No. GZC20241916) and the General Fund (grant No. 2024M763531) of the China Postdoctoral Science Foundation. L.L.Z. acknowledges the support by the Foundation of Guilin University of Technology (No. RD2500000384). This work used data supplied by the UK Swift Science Data Centre at the University of Leicester and data obtained with Einstein Probe.

APPENDIX

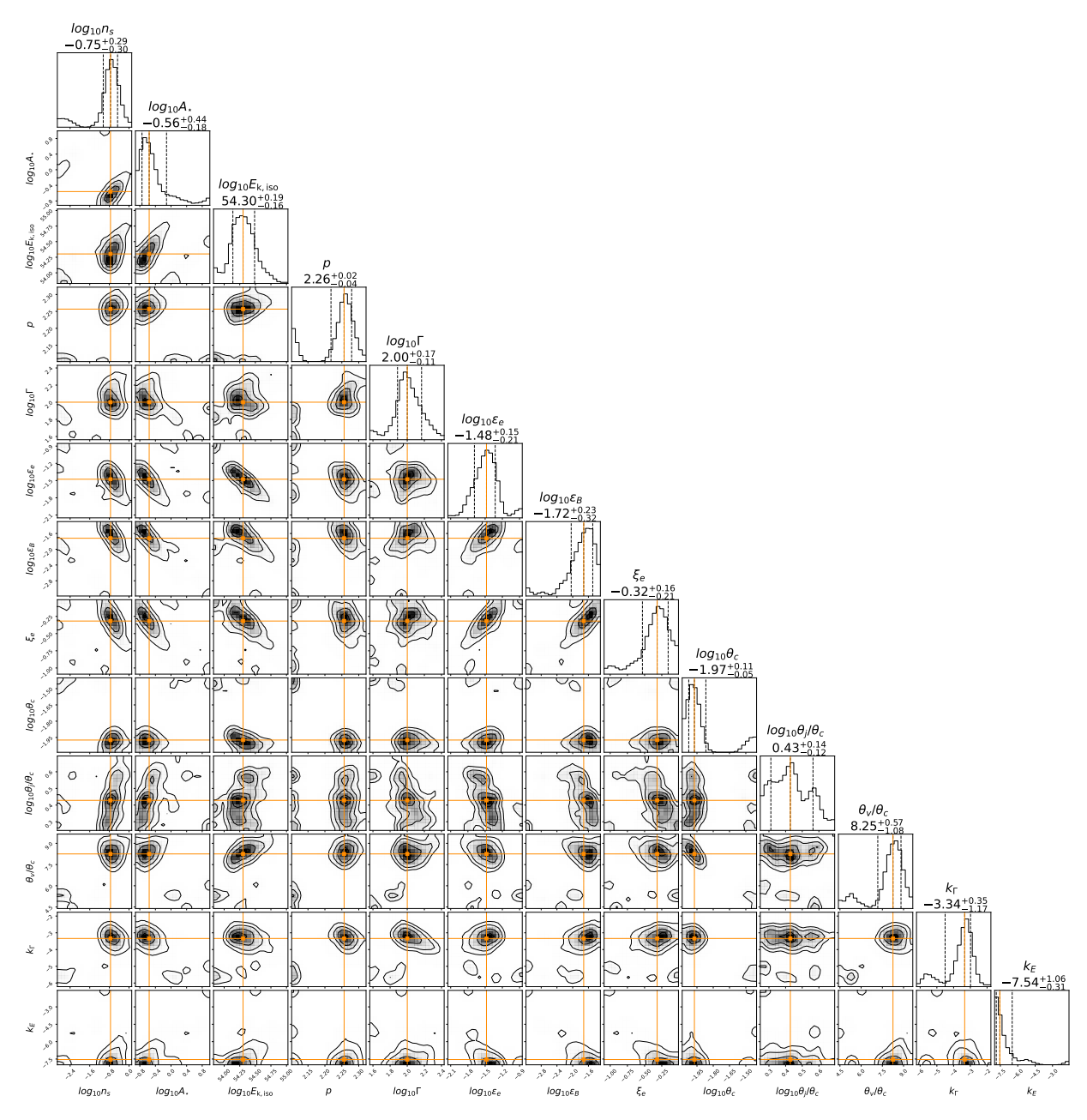


Figure 4. Corner plot of the MCMC posterior sample density distributions of EP240414a.

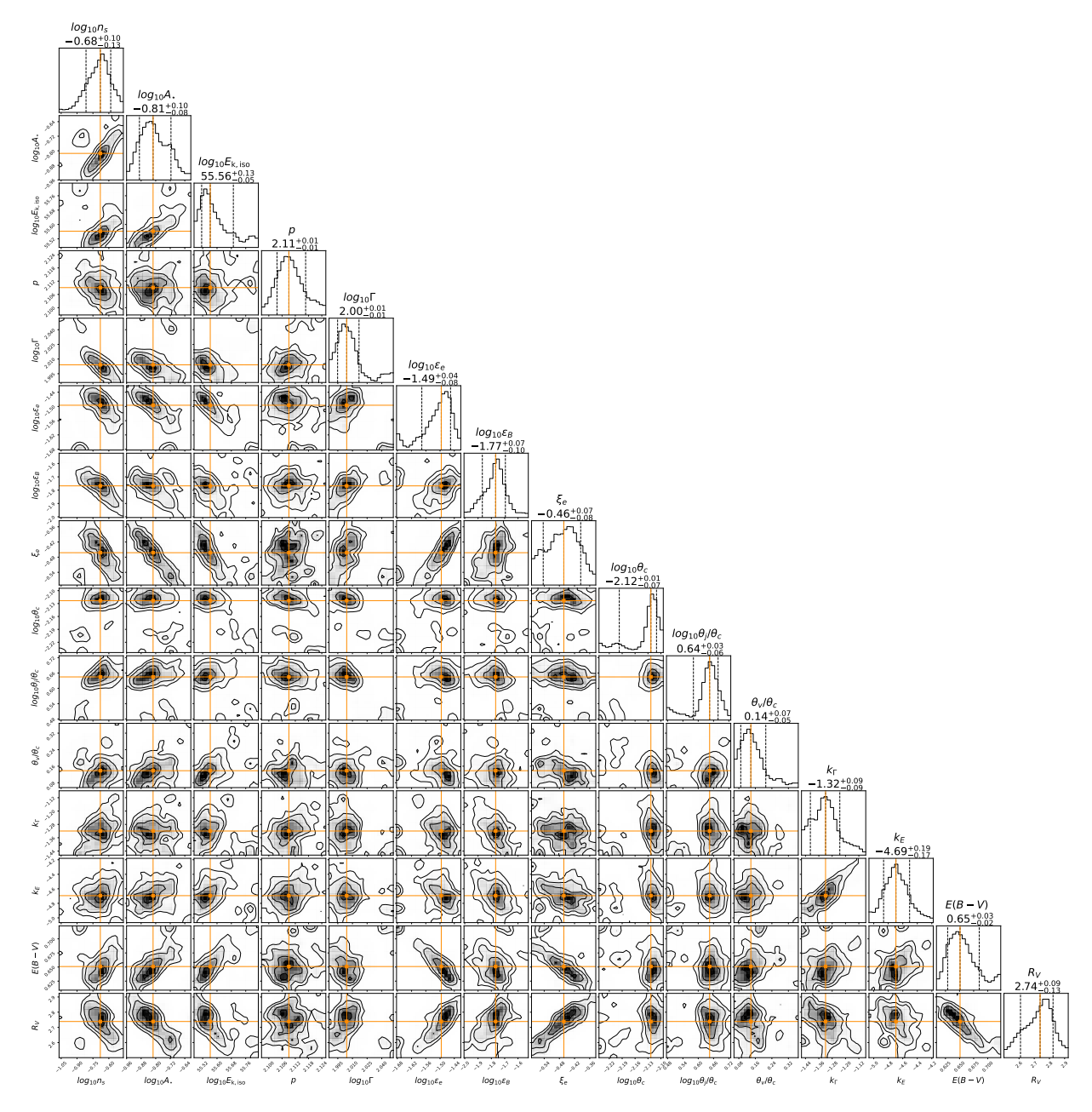


Figure 5. Corner plot of the MCMC posterior sample density distributions of GRB 240529A.

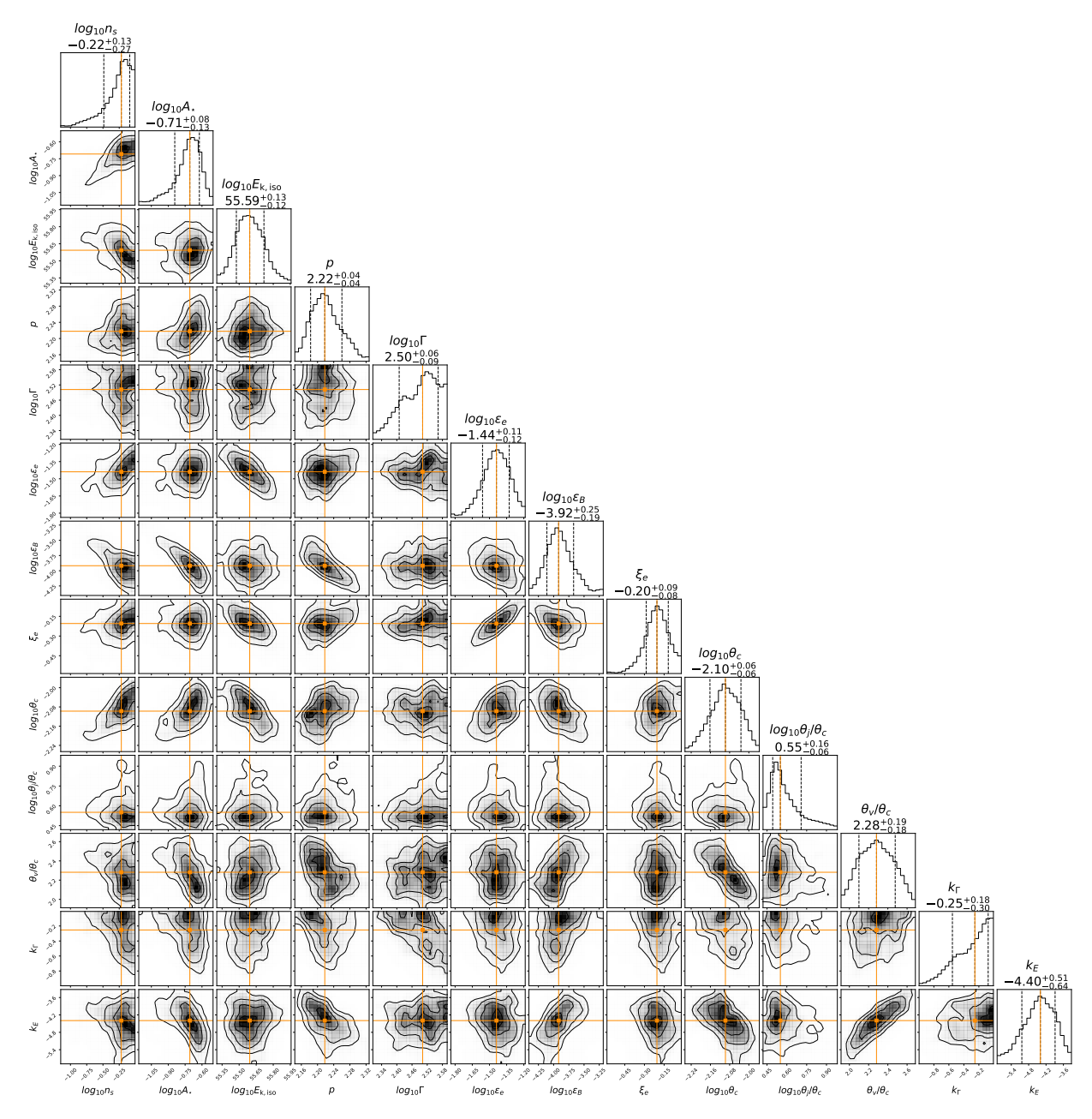


Figure 6. Corner plot of the MCMC posterior sample density distributions of GRB 240218A.

REFERENCES

- Barbary, K. 2016, extinction v0.3.0, Zenodo, doi: 10.5281/zenodo.804967
- Beniamini, P., Granot, J., & Gill, R. 2020, MNRAS, 493, 3521, doi: 10.1093/mnras/staa538
- Björnsson, G., Gudmundsson, E. H., & Jóhannesson, G. 2004, ApJL, 615, L77, doi: 10.1086/426477
- Bright, J. S., Carotenuto, F., Fender, R., et al. 2025, ApJ, 981, 48, doi: 10.3847/1538-4357/adaaef
- Brivio, R., Campana, S., Covino, S., et al. 2025, A&A, 695, A239, doi: 10.1051/0004-6361/202452748
- Busmann, M., O'Connor, B., Sommer, J., et al. 2025, arXiv e-prints, arXiv:2503.14588, doi: 10.48550/arXiv.2503.14588
- Castor, J., McCray, R., & Weaver, R. 1975, ApJL, 200, L107, doi: 10.1086/181908
- Chen, H.-W., Prochaska, J. X., Ramirez-Ruiz, E., et al. 2007, ApJ, 663, 420, doi: 10.1086/518111
- Chevalier, R. A., & Li, Z.-Y. 2000, ApJ, 536, 195, doi: 10.1086/308914
- Chevalier, R. A., Li, Z.-Y., & Fransson, C. 2004, ApJ, 606, 369, doi: 10.1086/382867
- Chrimes, A. A., Gompertz, B. P., Kann, D. A., et al. 2022, MNRAS, 515, 2591, doi: 10.1093/mnras/stac1796
- Dai, Z. G., & Lu, T. 2002, ApJL, 565, L87, doi: 10.1086/339418
- Dai, Z. G., & Wu, X. F. 2003, ApJL, 591, L21, doi: 10.1086/377037
- Eldridge, J. J., Genet, F., Daigne, F., & Mochkovitch, R. 2006, MNRAS, 367, 186, doi: 10.1111/j.1365-2966.2005.09938.x
- Falcone, A. D., Burrows, D. N., Lazzati, D., et al. 2006, ApJ, 641, 1010, doi: 10.1086/500655
- Filgas, R., Krühler, T., Greiner, J., et al. 2011, A&A, 526, A113, doi: 10.1051/0004-6361/201015320
- Foreman-Mackey, D. 2016, The Journal of Open Source Software, 1, 24, doi: 10.21105/joss.00024
- Foreman-Mackey, D., Hogg, D. W., Lang, D., & Goodman, J. 2013, \pasp, 125, 306, doi: 10.1086/670067
- Fraija, N., Dichiara, S., Pedreira, A. C. C. d. E. S., et al. 2019, ApJL, 879, L26, doi: 10.3847/2041-8213/ab2ae4
- Fraija, N., Veres, P., Zhang, B. B., et al. 2017, ApJ, 848, 15, doi: 10.3847/1538-4357/aa8a72
- Galama, T. J., Vreeswijk, P. M., van Paradijs, J., et al. 1998, Nature, 395, 670, doi: 10.1038/27150
- Gat, I., van Eerten, H., & MacFadyen, A. 2013, ApJ, 773, 2, doi: 10.1088/0004-637X/773/1/2
- Gendre, B., Galli, A., Corsi, A., et al. 2007, A&A, 462, 565, doi: 10.1051/0004-6361:20065220

- Geng, J. J., Wu, X. F., Huang, Y. F., Li, L., & Dai, Z. G. 2016, ApJ, 825, 107, doi: 10.3847/0004-637X/825/2/107
- Geng, J. J., Wu, X. F., Huang, Y. F., & Yu, Y. B. 2013, ApJ, 779, 28, doi: 10.1088/0004-637X/779/1/28
- Geng, J. J., Wu, X. F., Li, L., Huang, Y. F., & Dai, Z. G. 2014, ApJ, 792, 31, doi: 10.1088/0004-637X/792/1/31
- Geng, J.-J., Hu, D.-F., Gao, H.-X., et al. 2025, ApJL, 984, L65, doi: 10.3847/2041-8213/add00e
- Gianfagna, G., Piro, L., Bruni, G., et al. 2025, arXiv e-prints, arXiv:2505.05444, doi: 10.48550/arXiv.2505.05444
- Gillanders, J. H., Rhodes, L., Srivastav, S., et al. 2024, ApJL, 969, L14, doi: 10.3847/2041-8213/ad55cd
- Gottlieb, O. 2025, arXiv e-prints, arXiv:2509.04551, doi: 10.48550/arXiv.2509.04551
- Gottlieb, O., Bromberg, O., Singh, C. B., & Nakar, E. 2020, MNRAS, 498, 3320, doi: 10.1093/mnras/staa2567
- Granot, J., Nakar, E., & Piran, T. 2003, Nature, 426, 138, doi: 10.1038/426138a
- Granot, J., & Sari, R. 2002, ApJ, 568, 820, doi: 10.1086/338966
- Greiner, J., Klose, S., Salvato, M., et al. 2003, ApJ, 599, 1223, doi: 10.1086/379606
- Guidorzi, C., Monfardini, A., Gomboc, A., et al. 2005, ApJL, 630, L121, doi: 10.1086/491655
- Hamidani, H., & Ioka, K. 2021, MNRAS, 500, 627, doi: 10.1093/mnras/staa3276
- Hamidani, H., Sato, Y., Kashiyama, K., et al. 2025, ApJL, 986, L4, doi: 10.3847/2041-8213/add99d
- Harris, C. R., Millman, K. J., van der Walt, S. J., et al. 2020, Nature, 585, 357, doi: 10.1038/s41586-020-2649-2
- Heyl, J. S., & Perna, R. 2003, ApJL, 586, L13, doi: 10.1086/374652
- Hou, S. J., Geng, J. J., Wang, K., et al. 2014, ApJ, 785, 113, doi: 10.1088/0004-637X/785/2/113
- Huang, Y. F., Wu, X. F., Dai, Z. G., Ma, H. T., & Lu, T. 2004, ApJ, 605, 300, doi: 10.1086/382202
- Hunter, J. D. 2007, Computing in Science and Engineering, 9, 90, doi: 10.1109/MCSE.2007.55
- Jin, Z. P., Xu, D., Covino, S., et al. 2009, MNRAS, 400, 1829, doi: 10.1111/j.1365-2966.2009.15555.x
- Kamble, A., Resmi, L., & Misra, K. 2007, ApJL, 664, L5, doi: 10.1086/520533
- Kong, S. W., Wong, A. Y. L., Huang, Y. F., & Cheng,K. S. 2010, MNRAS, 402, 409,doi: 10.1111/j.1365-2966.2009.15886.x
- Laskar, T., Berger, E., Margutti, R., et al. 2015, ApJ, 814, 1, doi: 10.1088/0004-637X/814/1/1

- Lazzati, D., Rossi, E., Covino, S., Ghisellini, G., & Malesani, D. 2002, A&A, 396, L5, doi: 10.1051/0004-6361:20021618
- Levan, A. J., Jonker, P. G., Saccardi, A., et al. 2024, arXiv e-prints, arXiv:2404.16350,
 - doi: 10.48550/arXiv.2404.16350
- Li, L., Wang, X.-G., Zheng, W., et al. 2020, ApJ, 900, 176, doi: 10.3847/1538-4357/aba757
- Li, X.-Y., Lin, D.-B., Ren, J., et al. 2021, ApJ, 922, 22, doi: 10.3847/1538-4357/ac1ff2
- Liang, E.-W., Li, L., Gao, H., et al. 2013, ApJ, 774, 13, doi: 10.1088/0004-637X/774/1/13
- Monfardini, A., Kobayashi, S., Guidorzi, C., et al. 2006, ApJ, 648, 1125, doi: 10.1086/506170
- Nakar, E., Ando, S., & Sari, R. 2009, The Astrophysical Journal, 703, 675, doi: 10.1088/0004-637X/703/1/675
- Nakar, E., & Granot, J. 2007, MNRAS, 380, 1744, doi: 10.1111/j.1365-2966.2007.12245.x
- Nardini, M., Greiner, J., Krühler, T., et al. 2011, A&A, 531, A39, doi: 10.1051/0004-6361/201116814
- Nardini, M., Elliott, J., Filgas, R., et al. 2014, A&A, 562, A29, doi: 10.1051/0004-6361/201321525
- Nava, L., Sironi, L., Ghisellini, G., Celotti, A., & Ghirlanda, G. 2013, Monthly Notices of the Royal Astronomical Society, 433, 2107, doi: 10.1093/mnras/stt872
- Panaitescu, A., Mészáros, P., & Rees, M. J. 1998, ApJ, 503, 314, doi: 10.1086/305995
- Pe'er, A., & Wijers, R. A. M. J. 2006, ApJ, 643, 1036, doi: 10.1086/500969
- Planck Collaboration, Ade, P. A. R., Aghanim, N., et al. 2016, 594, A13, doi: 10.1051/0004-6361/201525830
- Ramirez-Ruiz, E., Dray, L. M., Madau, P., & Tout, C. A. 2001, MNRAS, 327, 829,
 - doi: 10.1046/j.1365-8711.2001.04762.x
- Ramirez-Ruiz, E., García-Segura, G., Salmonson, J. D., & Pérez-Rendón, B. 2005, ApJ, 631, 435, doi: 10.1086/432433
- Ramirez-Ruiz, E., & MacFadyen, A. I. 2010, ApJ, 716, 1028, doi: 10.1088/0004-637X/716/2/1028
- Rastinejad, J. C., Levan, A. J., Jonker, P. G., et al. 2025, ApJL, 988, L13, doi: 10.3847/2041-8213/ade7f9
- Rees, M. J., & Mészáros, P. 1998, ApJL, 496, L1, doi: 10.1086/311244
- Ren, J., Wang, Y., & Dai, Z.-G. 2024, ApJ, 962, 115, doi: 10.3847/1538-4357/ad1bcd
- Sari, R., Piran, T., & Narayan, R. 1998, ApJL, 497, L17, doi: 10.1086/311269
- Scalo, J., & Wheeler, J. C. 2001, ApJ, 562, 664, doi: 10.1086/323858

- Shu, X., Yang, L., Yang, H., et al. 2025, ApJL, 990, L29, doi: 10.3847/2041-8213/adf4cd
- Srivastav, S., Chen, T. W., Gillanders, J. H., et al. 2025, ApJL, 978, L21, doi: 10.3847/2041-8213/ad9c75
- Starling, R. L. C., Wijers, R. A. M. J., Hughes, M. A., et al. 2005, MNRAS, 360, 305, doi: 10.1111/j.1365-2966.2005.09042.x
- Sun, H., Zhang, B., & Li, Z. 2015, ApJ, 812, 33, doi: 10.1088/0004-637X/812/1/33
- Sun, H., Li, W. X., Liu, L. D., et al. 2025, Nature Astronomy, 9, 1073, doi: 10.1038/s41550-025-02571-1
- Sun, T.-R., Geng, J.-J., Yan, J.-Z., et al. 2024, ApJL, 976, L20, doi: 10.3847/2041-8213/ad85da
- Svinkin, D., Frederiks, D., Ulanov, M., et al. 2024, GRB Coordinates Network, 36584, 1
- Tam, P. H., Pun, C. S. J., Huang, Y. F., & Cheng, K. S. 2005, NewA, 10, 535, doi: 10.1016/j.newast.2005.03.003
- Tchekhovskoy, A., McKinney, J. C., & Narayan, R. 2008, MNRAS, 388, 551, doi: 10.1111/j.1365-2966.2008.13425.x
- The Astropy Collaboration, Robitaille, T. P., Tollerud, E. J., et al. 2013, Astronomy & Astrophysics, 558, A33, doi: 10.1051/0004-6361/201322068
- Tian, X., Qin, Y., Du, M., Yi, S.-X., & Tang, Y.-K. 2022, ApJ, 925, 54, doi: 10.3847/1538-4357/ac3de4
- van Dalen, J. N. D., Levan, A. J., Jonker, P. G., et al. 2025, ApJL, 982, L47, doi: 10.3847/2041-8213/adbc7e
- van Eerten, H. J., Leventis, K., Meliani, Z., Wijers,
 R. A. M. J., & Keppens, R. 2010, MNRAS, 403, 300,
 doi: 10.1111/j.1365-2966.2009.16109.x
- van Eerten, H. J., Meliani, Z., Wijers, R. A. M. J., & Keppens, R. 2009, MNRAS, 398, L63, doi: 10.1111/j.1745-3933.2009.00711.x
- van Marle, A. J., Langer, N., Yoon, S. C., & García-Segura,
 G. 2008, A&A, 478, 769,
 doi: 10.1051/0004-6361:20078802
- Virtanen, P., Gommers, R., Oliphant, T. E., et al. 2020, Nature Methods, 17, 261, doi: 10.1038/s41592-019-0686-2
- Waxman, E. 1997, The Astrophysical Journal, 491, L19, doi: 10.1086/311057
- Woosley, S. E., & Bloom, J. S. 2006, ARA&A, 44, 507, doi: 10.1146/annurev.astro.43.072103.150558
- Wu, G.-L., Yu, Y.-W., Liu, L.-D., et al. 2025, arXiv e-prints, arXiv:2505.12491, doi: 10.48550/arXiv.2505.12491
- Yadav, M., Troja, E., Ricci, R., et al. 2025, arXiv e-prints, arXiv:2505.08781, doi: 10.48550/arXiv.2505.08781
- Yi, S.-X., Wu, X.-F., & Dai, Z.-G. 2013, ApJ, 776, 120, doi: 10.1088/0004-637X/776/2/120
- Yi, S.-X., Wu, X.-F., Zou, Y.-C., & Dai, Z.-G. 2020, ApJ, 895, 94, doi: 10.3847/1538-4357/ab8a53

Yu, Y. B., Huang, Y. F., Wu, X. F., Xu, M., & Geng, J. J. 2015, ApJ, 805, 88, doi: 10.1088/0004-637X/805/2/88

Yu, Y. W., & Dai, Z. G. 2007, A&A, 470, 119, doi: 10.1051/0004-6361:20077053

Zhang, B. 2018, The physics of gamma-ray bursts (Cambridge University Press),

doi: 10.1017/9781139226530

Zhang, B., & Mészáros, P. 2002, ApJ, 566, 712, doi: 10.1086/338247

—. 2004, International Journal of Modern Physics A, 19, 2385, doi: 10.1142/S0217751X0401746X

Zhang, B., Wang, X.-Y., & Zheng, J.-H. 2024, Journal of High Energy Astrophysics, 41, 42, doi: 10.1016/j.jheap.2024.01.002

Zhang, B.-B., Liang, E.-W., & Zhang, B. 2007, ApJ, 666, 1002, doi: 10.1086/519548

Zheng, J.-H., Zhu, J.-P., Lu, W., & Zhang, B. 2025, ApJ, 985, 21, doi: 10.3847/1538-4357/adc993